ACS SENSORS

pubs.acs.org/acssensors

Article



# Demonstrating the Analytical Potential of a Wearable Microneedle-Based Device for Intradermal $CO_2$ Detection

Águeda Molinero-Fernandez, Qianyu Wang, Xing Xuan, Åsa Konradsson-Geuken, Gastón A. Crespo,* and María Cuartero*

Cite This: *ACS Sens.* 2024, 9, 361−370

Read Online

ACCESS | Metrics & More | Article Recommendations | Supporting Information

**ABSTRACT:** Monitoring of carbon dioxide ($CO_2$) body levels is crucial under several clinical conditions (e.g., human intensive care and acid−base disorders). To date, painful and risky arterial blood punctures have been performed to obtain discrete $CO_2$ measurements needed in clinical setups. Although noninvasive alternatives have been proposed to assess $CO_2$, these are currently limited to benchtop devices, requiring trained personnel, being tedious, and providing punctual information, among other disadvantages. To the best of our knowledge, the literature and market lack a wearable device for real-time, on-body monitoring of $CO_2$. Accordingly, we have developed a microneedle (MN)-based sensor array, labeled as $CO_2$−MN, comprising a combination of potentiometric pH- and carbonate ($CO_3^{2-}$)-selective electrodes together with the reference electrode. The $CO_2$−MN is built on an epidermal patch that allows it to reach the stratum corneum of the skin, measuring pH and $CO_3^{2-}$ concentrations directly into the interstitial fluid (ISF). The levels for the pH−$CO_3^{2-}$ tandem are then used to estimate the $PCO_2$ in the ISF. Assessing the response of each individual MN, we found adequate response time ($t_{95}$ < 5s), sensitivity (50.4 and −24.6 mV dec$^{-1}$ for pH and $CO_3^{2-}$, respectively), and stability (1.6 mV h$^{-1}$ for pH and 2.1 mV h$^{-1}$ for $CO_3^{2-}$). We validated the intradermal measurements of $CO_2$ at the ex vivo level, using pieces of rat skin, and then, with in vivo assays in anesthetized rats, showing the suitability of the $CO_2$−MN wearable device for on-body measurements. A good correlation between ISF and blood $CO_2$ concentrations was observed, demonstrating the high potential of the developed MN sensing technology as an alternative to blood-based analysis in the near future. Moreover, these results open new horizons in the noninvasive, real-time monitoring of $CO_2$ as well as other clinically relevant gases.

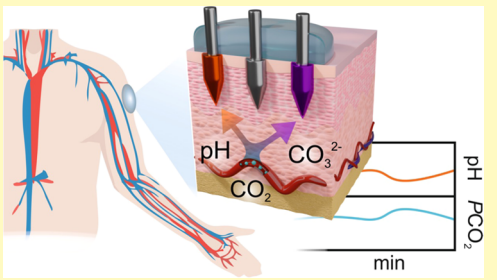


**KEYWORDS:** *ion-selective microneedles, $CO_2$ sensing, wearable sensor, interstitial fluid, in vivo measurements, blood correlation*



The blood gas analysis is a standard diagnostic tool widely used in intensive care units (ICUs). It provides information about the health status of a patient concerning certain respiratory, circulatory, and metabolic disorders.[1] Typically, this kind of blood analysis can be performed in any circulatory system (artery, vein, and capillary), providing different types of information, but the most common practice implies arterial blood, resulting in the well-known arterial blood gas (ABG) analysis that grants knowledge related to the respiratory system. The ABG is a very invasive and painful method for adults and indeed unfeasible in neonates, owing to the small blood volume of the newborn.[2] Despite ABG being the gold standard for the clinical analysis of pH and partial pressures of oxygen and carbon dioxide ($PO_2$ and $PCO_2$, respectively), the results are not immediately available because of the blood collection and analysis, which require high levels of expertise from the clinical staff.[3]

About the sampling procedure, once the arterial blood is obtained via an arterial puncture with special needle and syringe, the following main aspects must be considered to avoid any alteration of the blood, and therefore, inaccurate information: (i) unintentional exposure to the air, (ii) in vitro coagulation, (iii) inappropriate selection of the sample container, (iv) optimal temperature for sample storage, (v) the calibration of the analytical instrument (electrochemical sensors composing the ABG instrument) by lab experts, and (vi) the time from the sample collection to its analysis must not exceed the range from 15 to 30 min.[4] Thus, the entire process is laborious, expensive, slow (single information per day or even lower frequency), with the outcomes being highly dependent on the collection and storage of the sample, as well as calibration condition of the analytical instrument.[5] Importantly, ICU patients usually require frequent blood gas testing (every second hour in same cases): the most common option for this monitoring is arterial catheterization, which is

Received: October 3, 2023
Revised: November 29, 2023
Accepted: December 18, 2023
Published: January 4, 2024

known to be associated with severe complications, such as arterial/nervous lesions, ischemia, and infections.[5]

From the clinical point of view, the capillary blood (1−2 mm in depth from the skin) and the interstitial fluid (ISF, less than 1 mm in depth from the skin) have been shown to contain significant information about the physiological status of the individual.[6] Moreover, few systematic studies, mainly focused on glucose, have attempted to discover reliable composition correlations between the bloodstream and those two biological fluids.[6] In such a context, clinical trials involving pediatric scenarios showed that capillary blood gas (CBG) analysis effectuated at specific conditions may be an alternative for ABG.[7] Other studies have pointed out that pH and $PCO_2$ measurements correlate well in venous, arterial, and capillary blood, whereas $PO_2$ lacks any correlation.[8] Nonetheless, all of these studies should be carefully considered due to the high risk of change in the gas content of the blood during the entire analysis process.

In a different direction, noninvasive methods for $CO_2$ detection have been developed to overcome the above-mentioned issues related to ABG (and analogous techniques applied to other blood samples), such as the end-tidal approach, a colorimetric $CO_2$ detector for exhalated air and transcutaneous $CO_2$ ($tcCO_2$) measurements, though all of these exhibit important applicability limitations yet.[5] Regarding $tcCO_2$, the amount of $CO_2$ diffusing through the skin is detected. Briefly, the sensor, which is a pH electrode in contact with a solution delimited by a thin $CO_2$ permeable membrane (Stow−Severinghaus electrode), is placed onto the skin surface. The $CO_2$ that diffuses across the skin (after warming) passes through the membrane and dissolves in the solution, causing a pH change that is registered by the pH electrode. The $tcCO_2$ technique is painless, without the necessity of blood extraction, and has also presented a good correlation with ABG values.[5] However, the precision of the measurements has been questioned from data obtained in certain setups, such as emergency rooms and ICUs. The need for warming the skin at above 42 °C results in both skin burns (especially in neonates) and deterioration of the sensor itself.[9] The need for continuous recalibration (every few hours in some cases), given the low stability of the sensor over time, is another inconvenience.[9]

Considering sensing devices capable of working under the stratum corneum of the skin, microneedle (MN) technology has been positioned as an elegant approach for measuring in the ISF. Even though significant progress has been recently demonstrated in MN-based electrochemical sensors (by our group and others[10−15]), its implementation for gas monitoring remains underexplored. An example found in the literature is based indeed on an optical MN for intradermal $O_2$ monitoring in pig skin.[16] To the best of our knowledge, neither electrochemical nor optical MNs have been proposed for the assessment of $PCO_2$ so far. Herein, we present the development of a new MN-based sensing concept for the minimally invasive transdermal detection of $CO_2$. It is a potentiometric $CO_2$−MN system that consists of three all-solid-state ion-selective MNs: a carbonate-selective MN ($CO_3^{2-}$−MN), a pH-selective MN (pH−MN), and a reference MN (RE−MN). When implemented in an epidermal patch, the $CO_2$−MN system penetrates the stratum corneum of the skin, measuring directly into the ISF and without the need of generating $CO_2$ diffusion, in contrast to the $tcCO_2$ method. Having simultaneous measurements of pH and $CO_3^{2-}$ in the ISF, concentrations of bicarbonate and $PCO_2$ can be estimated. Accordingly, this work demonstrates the accurate detection of $PCO_2$ in ISF with a potentiometric MN−$CO_2$ system, including the in vivo feasibility demonstration with anesthetized rats. Also, the correlation between blood and ISF $CO_2$ measurements is assessed to investigate the potential to substitute ABG in clinical settings in the near future.

## EXPERIMENTAL SECTION

**Reagents and Materials.** Hydrogen ionophore I (tridodecylamine) of selectophore grade, carbonate ionophore VII (*N*,*N*-dioctyl-3$\alpha$,12$\alpha$-bis(4-trifluoroacetylbenzoyloxy)-5$\beta$-cholan-24-amide) of selectophore grade, poly(vinyl chloride) (PVC), polyurethane (PU) (Reference 81367, selectophore grade), bis(2-ethylhexyl)sebacate (DOS, >97%), sodium tetrakis[3,5-bis(trifluoromethyl)phenyl]borate (NaTFPB), tridodecylmethylammonium chloride (TDMACl), bis(2-ethylhexyl) adipate (DEHA), and tetrahydrofuran (THF, >99.9%) were purchased from Sigma-Aldrich (Sweden). Carbon/graphite ink (C2030519P4) and silver/silver chloride (Ag/AgCl) 50/50 paste (C2131007D3) were obtained from Sunchemical.[17,18] Silicon rubber (Ecoflex 00−50 platinum cure) and stainless-steel microneedles (MN) (Dermaroller local supplier, Sweden) were employed for the fabrication of the MN patch. Other chemicals and materials are provided in the Supporting Information.

**Fabrication of the MN Patch for $CO_2$ Detection.** The $CO_2$−MN patch consisted of a flexible substrate made of a 1 mm deep silicone rubber in which three solid stainless-steel MNs (1500 $\mu$m in length and 150 $\mu$m in diameter) were placed and then conveniently modified: the upper MN part was used to make the electrical connections to the reader (potentiometer), while the tip part (500 $\mu$m in length after being fixed in the substrate) was conveniently modified to provide the sensing capabilities. Two of the MNs were modified to create two working electrodes (WE−MNs) consisting of ion-selective electrodes with plasticized polymeric membranes that are selective for pH or $CO_3^{2-}$. Then, the third MN was modified to provide a common reference electrode (RE−MN) for the potentiometric measurements. Both WEs were of the all-solid-state format, prepared with three layers deposited onto the stainless-steel MN structure. From the inside to outside part: (i) a carbon ink layer to improve the conductivity of the MN and the adherence of the next layer to the MN; (ii) lipophilic (functionalized) multiwalled carbon nanotubes (f-MWCNTs)[14] as the ion-to-electron transducer; and (iii) the corresponding ion-selective membrane (ISM) to provide selectivity and the potential response. The RE-MN was also of the all-solid-state format and consisted of an Ag/AgCl layer covered by a reference membrane (RM) and an external PU layer, as reported elsewhere.[14]

Figure 1 depicts a scheme of all of the steps accomplished toward the preparation of the MN-$CO_2$ wearable patch. First, the tips of the two MNs to be used as the WEs were covered by a film of carbon by dip-coating them into a commercial ink. A similar procedure was followed to prepare the RE-MN but covering the MN with Ag/AgCl. The three MNs were cured in an oven at 120 °C for 10 min. Then, the three (coated) MNs were inserted into the substrate, and the upper part of each MN was glued to the rubber with Loctite Super Glue (Henkel Norden AB). After drying the glue for 20 min at room temperature, the remaining functionalization steps were accomplished in the tip part of each (coated) MN.

For the WEs, 10 subsequent layers with a volume of 2 $\mu$L of an f-MWCNTs dispersion in THF (1 mg $mL^{-1}$) were drop-cast onto the carbon MN.[10,14] Drying steps of 4 min were performed between layers. The excess of f-MWCNTs after each drop deposition was carefully wiped off using a micropipette. Then, 3 layers of a volume of 1 $\mu$L of the corresponding ISM (the compositions of the cocktails are provided in the Supporting Information) were drop-cast. Drying steps of 20 min were performed after the addition of the first and second layers and 4 h after the deposition of the final layer to ensure the appropriate drying (i.e., THF evaporation) of the membrane. Finally, both WE−MNs were conditioned overnight. The pH-MN was conditioned in 1 mM HCl and the $CO_3^{2-}$−MN was conditioned in 1


https://doi.org/10.1021/acssensors.3c02086
ACS Sens. 2024, 9, 361−370

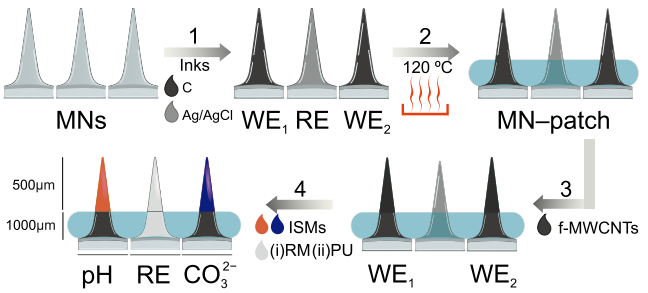


**Figure 1.** Scheme of the procedure for the preparation of the MN-$CO_2$ patch: (1) stainless-steel solid MNs are modified with commercial inks to obtain two WE-MNs and one RE-MN; (2) the MNs are cured in an oven and assembled into the silicon substrate; (3) deposition of f-MWCNTs on top of the carbon ink in the WE-MNs; (4) deposition of the corresponding ion-selective membrane (ISM) in the WE-MNs, and the reference membrane (RM) in the RE-MN, and deposition of an extrapolyurethane (PU) layer in the RE-MN.

mM $NaHCO_3$. For the RE, 3 layers of a volume of 1 $\mu$L of the reference membrane (RM) cocktail (see the composition in the Supporting Information), were drop-cast onto the Ag/AgCl MN. Drying steps of 20 min after the addition of the first and second layers and 4 h after the incorporation of the final layer were performed. Then, after overnight conditioning in a 3 M KCl solution, the RE was dried at room temperature for 1 h. An extra layer of PU (2 $\mu$L, 20 mg $mL^{-1}$ in THF) was drop-cast, and the MN was conditioned in 3 M KCl for 12 h.

**Ex Vivo Measurements in Pieces of Rat Skin.** For the ex vivo experiments, 6 pieces of rat skin (approximately 5 cm × 5 cm, Biobreeder rats) were overnight conditioned in solutions of artificial interstitial fluid (AISF) containing different, known concentrations of $CO_2$ (0.2–3 mM). After that, the corresponding piece of skin was placed into a plastic support and covered with a piece of parafilm with the same dimensions as the MN patch to allow for MN-$CO_2$ patch insertion while isolating the rest of the skin (Figure S1). The skin pieces were obtained from euthanized rats and were donated by the Karolinska Experimental Research and Imaging Centre (Karolinska Institutet, Stockholm, Sweden).

**In Vivo Measurements in Anesthetized Rats.** Five anesthetized rats were employed for in vivo assays (see the Supporting Information). Prior to in vivo measurements, each awake rat was placed into an anesthesia induction chamber for initial anesthesia (isoflurane/air mixture, 2–4 L/min, 4% of isoflurane). After that, each rat was placed in an anesthesia mask, and the isoflurane level was adjusted according to 2–4 L/min isoflurane/air 2–2.5% v/v during the experiments. Any change in the anesthesia composition was recorded. A heating pad was placed under the animal during the whole experiment, and artificial tears (Viscotears, Bausch Lomb Nordic, Stockholm, Sweden) were applied to the eyes of the rat to lubricate the ocular surface when tear production is reduced due to the anesthesia. A small part of the back of the rat was shaved and sterilized with ethanol for MN insertion.

In parallel to the anesthesia and rat preparation procedure, the MN-$CO_2$ patch was calibrated by a 3-point procedure in AISF background. Notably, the solutions' pH and $CO_2$ levels were checked with commercial sensors to be exactly incorporated in the calibration graphs. The pH meter (Metrohm, Sweden) and Severinghaus probe (ThermoFisher) were used for this purpose. Then, the skin of the rat was carefully pierced with the $CO_2$–MN patch and the data was recorded for approximately 2 min. After the on-body acquisition, the rat was physically euthanized, and a blood sample was collected from the incision in the neck and analyzed with a portable blood gas analyzer (i-Stat 1). These experiments were approved by and conducted in accordance with the Uppsala Committee on Ethics of Animals (Dnr 5.8.18- 18873/2018, DOUU-2020–025). More details on the procedures are provided in the Supporting Information.

## RESULTS AND DISCUSSION

**Principle for $CO_2$ Detection with the $CO_2$–MN Patch.** The $CO_2$–MN patch consisted of two WE–MNs, labeled as a pH–MN and $CO_3^{2-}$–MN, and a shared RE–MN. The three MN–based electrodes were embedded into a silicone rubber substrate with a circular shape (Ø = 1 mm) forming the final $CO_2$–MN patch (Figure 2a). The MNs were connected to a miniaturized custom-made multipotentiometer board for signal acquisition and processing, being in turn wirelessly connected to the user interface in a mobile phone through Bluetooth (Figure 2b). The portable board was placed inside a 3D-printed casing for protection and better handling once connected to the MNs. The user interface was a custom-made mobile app to display, analyze, and store the real-time potentiometric signals obtained by the $CO_2$–MN patch (Figure 2c). Figure S2a,b show real pictures of the $CO_2$–MN patch and the entire device (i.e., MNs attached to the electronic board) when on-body measurements were performed in anesthetized rats.

Figure 2d exemplifies the dynamic measurements of pH and $CO_3^{2-}$ with the MNs together with the calculated $PCO_2$ profile. Importantly, the $CO_2$ (and $PCO_2$) detection relies on the potentiometric signals independently provided by the pH–MN and the $CO_3^{2-}$–MN sensors, as the following explained. The potentiometric signal of each MN is proportional to the $H^+$ (pH) and $CO_3^{2-}$ concentrations in the sample (i.e., considering concentration equal to activity in the AISF or ISF background). Thereafter, $CO_2$ concentration can be estimated according to eq 1

$$c_{CO_2} = \frac{c_{CO_3^{2-}} (c_{H^+})^2}{K_{a1} K_{a2}} \quad (1)$$

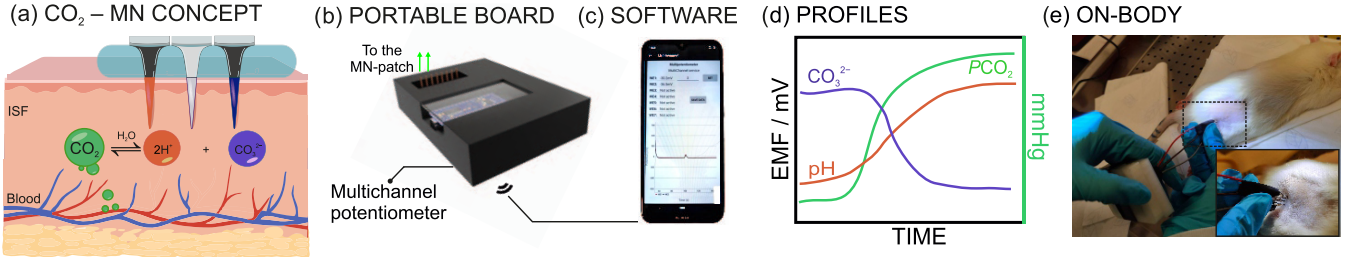


**Figure 2.** (a) Conceptual scheme of the $CO_2$–MN device and its working principle. (b) Image of the portable multichannel board embedded in a 3D-printed casing. (c) Custom-made software employed for the on-body measurements. (d) Dynamic profiles for pH and $CO_3^{2-}$ measured with the patch, and the $PCO_2$ profile calculated based on such measurements. (e) Image of on-body measurements in anesthetized rats.



https://doi.org/10.1021/acssensors.3c02086
ACS Sens. 2024, 9, 361–370

where $c_{co_3^{2-}}$ and $c_{H^+}$ are the $CO_3^{2-}$ and hydrogen-ion concentrations, respectively, and $K_{a1}$ and $K_{a2}$ are the first and second dissociation constants for carbonic acid. Then, it is known that the concentration of a gas dissolved in a liquid is proportional to the partial pressure of the gas under equilibrium conditions. Thus, $PCO_2$ can be obtained from the concentration of dissolved $CO_2$ using the following equation

$$CO_2 = s \times PCO_2 \quad (2)$$

where $s$ is the solubility constant for $CO_2$ in the medium.[19]

Notably, the use of two potentiometric probes to indirectly estimate the $CO_2$ levels was explored in various applications. For example, submergible probes based on $CO_3^{2-}$ and pH sensors were settled to monitor species of the carbon cycle in seawater.[20,21] Also, Kraig et al. demonstrated $CO_3^{2-}$ and pH inner-filling microelectrodes for the detection of $CO_2$ in the extracellular fluid of rat hippocampal slices,[22] and intracellular $CO_2$ measurements in skeletal muscle cells in anesthetized rats.[23] However, to the best of our knowledge, this sensing strategy has not yet been proposed for intradermal measurements with MNs in view of replacing ABG tests, as established in this work.

In view of executing proper on-body measurements in rats (Figure 2e), the MNs in the patch must reach the ISF while maintaining the integrity of the sensing elements and following a painless procedure for the individual. Effectively, the mechanical characteristics of the patch and the MNs (e.g., length of the MN, number of MNs, diameter at the MN base, diameter at the tip, and tip angle of the MN) influence both the piercing capabilities and the patient's comfort.[24] Accordingly, SEM images were acquired to investigate the suitability of the developed $CO_2$−MN patch for on-body measurements. The images are presented in Figure S3 in the Supporting Information. Both types of MNs, WE−MNs ($CO_3^{2-}$−MNs is depicted as an example) and the RE−MN, presented a length that ensures to reach the dermis (500 $\mu$m), a base diameter of <300 $\mu$m, tip diameter of <50 $\mu$m, and tip angle of <45°. These features agreed with already established thresholds for proper insertion into the skin while ensuring the user well-being.[24]

**In Vitro Characterization of the Analytical Performance of the MNs for pH and $CO_3^{2-}$ Detection.** First, the analytical performances of the MNs for the detection of pH and $CO_3^{2-}$ were studied by means of an in vitro configuration. The potentiometric responses at varying pH and $CO_3^{2-}$ concentrations were recorded for the corresponding WE-MN fixed in the patch and against a commercial double-junction Ag/AgCl reference electrode. Buffer solutions in the pH range from 5.0 to 8.5 were used to calibrate the pH-MN. For $CO_3^{2-}$, solutions with increasing concentrations of $NaHCO_3$ were prepared at pH = 7.4 (HEPES buffer background), in agreement with the physiological pH. Notably, the pH of the solutions was constantly monitored with the pH meter, and the final $CO_3^{2-}$ concentrations were calculated according to the acidic constants established for $H_2CO_3$ at 25 °C in water ($pK_{a1}$ 6.35 and $pK_{a2}$ 10.33).[25]

Close-to-Nernstian slopes were obtained for both WE-MNs: 53.9 ± 1.0 mV $pH^{-1}$ for pH ($n$ = 3), and −26.6 ± 0.5 mV $dec^{-1}$ for $CO_3^{2-}$ ($n$ = 3). The linear range of response (LRR) was observed from 5 to 8.5 for pH, which completely covers the expected values in ISF. Even though the arterial blood pH stays in the range of 7.35−7.45 under normal conditions, the pH of ISF seems to be more unstable and may vary in connection to some diseases. For example, acidic pHs (as low as 6.5) have been observed in diabetes and cancer clinical conditions, whereas alkaline pHs up to 8.5 have been reported for certain wounds.[26] The LRR for $CO_3^{2-}$ was obtained from 0.37 $\mu$M to 3 mM, which includes the levels expected in arterial and venous blood as well as ISF (Table S1). For both WEMNs, fast responses ($t_{95}$ < 5 s), good repeatability (RSD ≤ 2% for the slope and ≤1% for the intercept, 3 calibrations using the same MNs) and adequate between-electrodes reproducibility (RSD ≤ 4% for the slope and ≤25% for the intercept, 3 analogous MNs) were obtained (Table S2).

Next, we proceeded to substitute the commercial Ag/AgCl reference electrode by REMN, and the analytical parameters were re-evaluated. Advantageously, no significant changes were observed concerning the response of three analogous patches (Table S3) beyond a change in the displayed potential range, which is inherent to the change in the RE nature and mainly affected the intercept values for the calibration graphs. Moreover, the stability of the response was evaluated in artificial solutions at fixed pH and $CO_3^{2-}$ concentrations (Figure S4), showing acceptable medium-term drifts over 7 h of 0.9 ± 1.1 mV $h^{-1}$ in phosphate buffer at pH 7.4 and −0.8 ± 2.3 mV $h^{-1}$ in 20 mM $NaHCO_3$, for pH and $CO_3^{2-}$ MNs, respectively. A selectivity study was performed by considering the major ions found in ISF (Table S4) that may interfere in the potentiometric response. Other components (such as urea, glucose, amino acids, lactate, and ascorbic acid) are not expected to affect the measurements. Selectivity coefficients were estimated by using the separate solution method (SSM), in which individual calibration graphs are obtained for both the potential interference and the primary analyte (pH or $CO_3^{2-}$ in our case). Notably, as previously established, these values have to be considered as "apparent", since the interferent ions did not present Nernstian slopes and the SSM is based in such an assumption.[27] A comparison of the estimated logarithmic selectivity coefficients with those theoretically required to perform potentiometric measurements in ISF without any expected interference revealed the suitability of the $CO_2$−MN patch for such measurements (Table S5). Moreover, the selectivity coefficients agreed well with those reported for other MNs for pH, as well as ISEs based on the same ionophores as those used herein. Additionally, calibration curves were carried out in AISF media, the composition of which is provided in the Supporting Information, for a complete matrix interference study. Figure 3a,b presents the results. No significant differences in the slopes were observed compared to the previous results in buffered background (−26.4 ± 0.8 mV $dec^{-1}$ and −51.2 ± 0.7 mV $pH^{-1}$), and similar LRRs were obtained (5.0−8.5 for pH, and $10^{-6.0}$−$10^{-2.6}$ M for $CO_3^{-2}$), covering the expected concentrations in ISF (Table S2). These results suggested that the developed MNs can be used for the further analysis of real ISF.

The ability of the MNs to accurately detect time-based fluctuations in the pH and $CO_3^{-2}$ was assessed. This is important to ensure continuous monitoring of the patient's state with the $CO_2$−MN device. A reversibility test was performed by subsequently decreasing and increasing the pH in the range from 8 to 5, and increasing and decreasing the $CO_3^{-2}$ concentration from $10^{-6.0}$ to $10^{-3.0}$ M. The registered dynamic potentials are depicted in Figure 3c,d, respectively. In both cases, the MNs displayed a fully reversible signal with a variation of the slope of about 2.4% (%RSD) for pH, and 1.6% for $CO_3^{-2}$, and variations for the intercept of 2.5% for pH and


https://doi.org/10.1021/acssensors.3c02086
ACS Sens. 2024, 9, 361−370

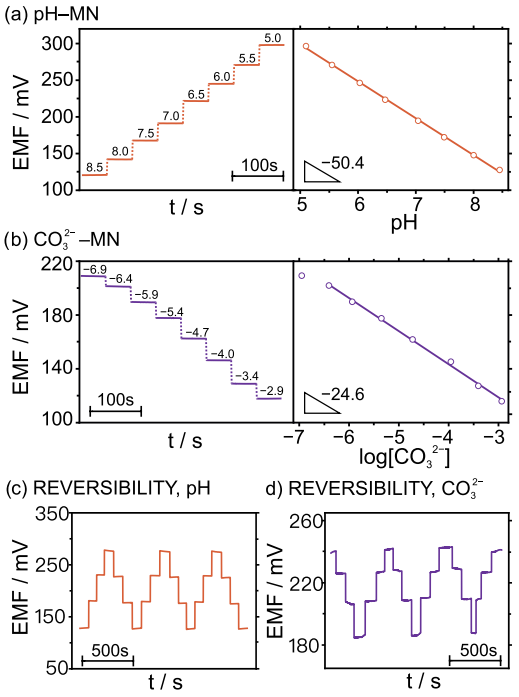


**Figure 3.** (a) Left: dynamic response of the pH–MN against the RE-MN at decreasing pH in the AISF background. Right: the corresponding calibration graph. (b) Left: dynamic response of $CO_3^{2-}$–MN against the RE–MN at increasing $CO_3^{2-}$ concentrations in the AISF background. Right: The corresponding calibration graph. (c, d) Reversibility study of the pH– and $CO_3^{2-}$–MN responses upon decreasing and increasing pH (8.0, 7.0, 6.0, and 5.0) and increasing and decreasing $CO_3^{2-}$ levels ($10^{-6.0}$, $10^{-5.0}$, $10^{-4.0}$, and $10^{-3.0}$ M) in the sample against the RE-MN.

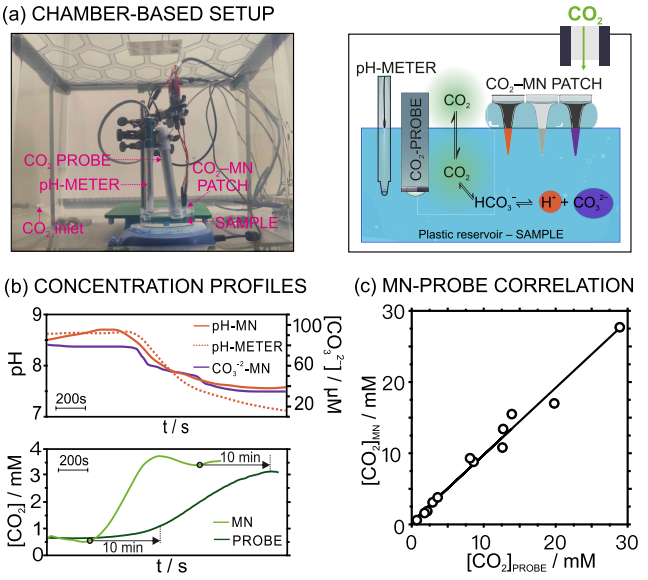


**Figure 4.** (a) Photo and scheme of the experimental setup for $CO_2$ monitoring in sample solutions placed inside the isolation chamber. (b) pH, $CO_3^{2-}$, and $CO_2$ dynamic profiles observed when the $CO_2$ concentration was increased inside the chamber. The $CO_2$–MN patch, pH meter, and Severinghaus probe were used to monitor the process. Dashed lines with arrows indicate the lag times for $CO_2$ measurements for the Severinghaus probe. (c) Correlation between the $CO_2$ values measured in artificial samples with the $CO_2$ MN patch and the Severinghaus probe ($n$ = 13).

2.7% for $CO_3^{-2}$. Notably, this study was conducted considering very wide concentration changes, which are not indeed expected to occur in real biological systems but served to fully understand the benefits and limitations of the developed $CO_2$–MN patch.

The stabilities of the MNs' responses were tested in AISF media over 7 h (see Figure S4). Higher drifts were observed in AISF than in buffer (2.1 ± 2.3 mV $h^{-1}$ for $CO_3^{2-}$ and 1.6 ± 0.4 mV $h^{-1}$ for pH). Regarding how these drifts could affect the accuracy of further on-body measurements, while a threshold of 10% in the $CO_2$ concentration is clinically accepted, which will be covered with the $CO_2$–MN patch over the first ca. 30 min, the drift may affect the system for relatively long assays (>1 h). Errors >20% may happen and therefore, recalibration every hour or the patch substitution could be a solution to avoid any inaccuracy issue, considering the case that such measurements are clinically relevant and therefore needed. Overall, the $CO_2$–MN patch presented excellent analytical features that are promising for reliable in vivo intradermal analysis of $CO_2$.

**In Vitro Investigation of the Determination of $CO_2$ from the pH–$CO_3^{2-}$ Measurements Obtained with the $CO_2$–MN Patch.** To demonstrate the possibility of monitoring real-time changes in $CO_2$ in both buffer and AISF samples, the $CO_2$–MN patch was tested in the setup presented in Figure 4a. In essence, the patch was immersed in a sample solution (25 mM $NaHCO_3$ or AISF), which is contained in a plastic reservoir, together with the commercial micro pH meter and the Severinghaus $CO_2$ probe. These two latter electrodes served to validate the profile of $CO_2$ levels calculated from the pH–$CO_3^{2-}$ tandem measurements. The $CO_2$ probe was positioned with a ca. 20° angle from the vertical to avoid the trapping of air bubbles at the tip of the electrode (as suggested by the supplier). The setup was in turn placed inside a plastic (isolation) chamber with a $CO_2$ gas inlet and outlet, and then the recording of all of the sensors was started. Notably, all of the sensors were calibrated out of the chamber before and after the experiment, in case of need for possible drift correction due to the long duration of the experiments. Once all of the sensors presented a stable signal in the sample solution (ca. after 100 s of having started the measurements), this was exposed to increasing $CO_2$ concentrations by introducing the gas into the chamber. The sample was allowed to re-equilibrate with the $CO_2$ partial pressure achieved in the atmosphere, while concentration changes were monitored by all of the sensors.

The dynamic $CO_2$ concentration in the solution was calculated according to eq 1, from the dynamic pH and the $CO_3^{2-}$ concentration provided by the MN patch. The top plot in Figure 4b shows the concentration profiles for pH and $CO_3^{2-}$ directly measured with the $CO_2$–MN patch, together with the estimated profile for $CO_2$, in one of the experiments performed in 25 mM $NaHCO_3$ solution (as an example). It was evidenced how the introduction of $CO_2$ into the chamber translated into a gradually higher $CO_2$ concentration in the sample solution, with decreasing pH and $CO_3^{2-}$ levels. Indeed, the pH profile agreed rather well with that displayed by the pH meter.

A comparison between the $CO_2$ profiles provided by the MN patch and the Severinghaus probe (the bottom plot in Figure 4b) revealed interesting hints. Despite both profiles being qualitatively similar, a slower response time of ca. 10 min was shown by the Severinghaus probe with respect to the MNs


https://doi.org/10.1021/acssensors.3c02086
ACS Sens. 2024, 9, 361−370

(illustrated with dashed arrows in Figure 4b). This is indeed expected since measurements based on the Severinghaus concept consider pH changes in the inner compartment of the probe, to which $CO_2$ is transported from the sample solution across a selective outer diffusion-limiting membrane.[5] Accordingly, the Severinghaus $CO_2$ probe may be utilized as a reference method to validate the $CO_2$ results provided by the MN patch only before and after the amount of $CO_2$ was increased in the sample solution, when both devices displayed constant and comparable responses considering a lag time of ca. 10 min.

Table S6 presents the $CO_2$ levels obtained by the $CO_2$−MN sensor and the commercial Severinghaus $CO_2$ probe after different increases in $CO_2$ concentration in both 25 mM $NaHCO_3$ solution and AISF. Notably, profiles and trends different from those just described for buffer samples (i.e., profiles in Figure 4b) were observed in AISF. In essence, phosphate species are the main factors responsible for the buffer capacity in the AISF (pH = 7.4) and thus, the addition of the $CO_2$ in the chamber induced an increase of the $HCO_3^-$ concentration without drastically affecting the (buffered) pH. Accordingly, there was an increase in the $HCO_3^-/H^+$ molar ratio that produced in turn an increase in the $CO_3^{2-}$ concentration (Figure S5) and hence, the $CO_2$.[28]

Overall, the differences between the outcomes from the $CO_2$−MN patch and the reference method were <15% (threshold established for the validation of an analytical methodology),[29,30] confirming the acceptable accuracy of the measurements. Larger differences were observed only in two samples, which indeed presented relatively high $CO_2$ concentrations (samples #8 and #15). Figure 4c shows the correlation between the $CO_2$ concentrations provided by the $CO_2$−MN patch and the $CO_2$ probe (sample size of $n$ = 13, without considering samples #8 and #15). A line with a $y$-intercept of 1.3 mM (rather close to zero), a slope of 0.8 (close to one), and a Pearson coefficient of 0.98 ($p$ < 0.05) were found, revealing the existence of a positive correlation. Despite these acceptable results, some aspects should be considered with regard to the evaluation/discussion of the $CO_2$-MN patch accuracy. On the one hand, at low $CO_2$ levels (0.1−0.5 mM), it has been reported that the precision of the Severinghaus probe is affected by a deviation from the (ideal) Nernstian response.[31] Effectively, there is a sensitivity worsening due to the deteriorating buffer capacity of the $HCO_3^-/CO_2$ couple, as already reported.[31] On the other hand, at high $CO_2$ levels, the corresponding $CO_3^{2-}$ concentration may be close to the lower LOD (i.e., 1.2 $\mu$M) of the $CO_3^{2-}$−MN, and hence, higher errors are likely to be obtained. Undoubtedly, the results demonstrated the feasibility and good reliability of measuring $CO_2$ with the $CO_2$−MN patch within the expected clinical range.

**Ex Vivo Analytical Characterization of the $CO_2$−MN Patch.** Two aspects were evaluated within the ex vivo assays: (i) the resilience of the MN sensors' response to skin insertion, and (ii) the accuracy of transdermal measurements of $CO_2$. First, the resiliency of the MN sensors when fixed in the patch was evaluated by comparing the corresponding calibration graphs before and after one and three insertions into pieces of rat skin. Although no significant changes were observed for the slopes (RSDs < 5%), a slight gradual shift of the intercept to a lower potential was displayed, being this change more significant after three insertions and in the case of the $CO_3^{2-}$−MN than for the pH−MN (Figure S6, RSDs of 8.7 and 5.9% for $CO_3^{2-}$ and pH). Accordingly, a recalibration of the MN sensors is advisable if the patch is desired to be used for more than one insertion.

In the second part of the study, the $CO_2$ contents in six pieces of rat skin that were 24-h-conditioned in solutions with different carbonate concentrations (200, 90, 50, 10 $\mu$M) and pHs (8.0, 7.7, 7.4, and 7.0) were transdermally detected with the MN patch. The setup described in the Experimental Section and Figure S1 was used in the experiments. The $CO_2$−MN patch was calibrated and then inserted into a skin sample, covered with a parafilm layer to shield the setup from the atmosphere, thus minimizing the diffusion of $CO_2$ across the skin. The transdermal $CO_3^{2-}$ concentration and pH were calculated from the potential readouts of the corresponding MN and calibration graphs. Finally, the $CO_2$ content was estimated from these two measurements, as explained in the previous section. In addition, the ISF inside each of the six skins was collected via a homemade extraction system composed of a hollow MN hub connected to a syringe pump (Figure S7) and analyzed with the reference techniques. Owing to the low volume of extracted ISF, the Severinghaus probe was not suitable for the validation of these measurements. Also, in most of the cases, the collected ISF volume was not enough for employing the portable blood gas analyzer device (Abbott i-Stat 1, a volume ≥95 $\mu$L is needed). Thus, the ISF samples were analyzed with a combination of an ultra-micro pH meter, and a $CO_3^{2-}$−MN, requiring ca. 5 $\mu$L of sample.

Figure 5 presents an example of the calibrations obtained for the pH− and $CO_3^{2-}$−MNs together with the dynamic potential profiles observed during the patch insertion in skin #5. As observed, the transdermal readouts presented by both MNs were rather constant at the experimental time scale of the skin insertion (ca. 2 min), and thus, the averaged potentials were extrapolated to the corresponding calibration graph for the calculation of pH, $CO_3^{2-}$ and $CO_2$ levels. The pH and the $CO_3^{2-}$ and $CO_2$ contents provided by the $CO_2$−MN patch were compared with those obtained by the reference methods in the analysis of the ISF samples collected from each skin. Table 1 displays all of the data as well as the differences (in %) between the MNs and the corresponding reference technique.

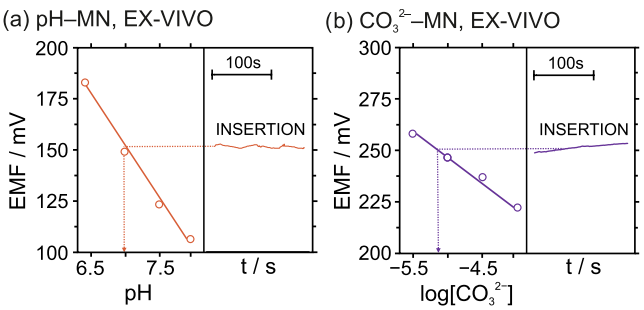


**Figure 5.** Calibration graphs and dynamic potentials observed for the (a) pH− and (b) $CO_3^{2-}$−MNs in the $CO_2$-MN patch performing the ex vivo experiments with skin #5.

Acceptable results were obtained for samples #2−#5, with averaged percentages for the differences of <20%: 0.9 ± 0.5 for pH, 14.2 ± 2.8 for $CO_3^{2-}$ and 10.3 ± 9.7 for $CO_2$. Additionally for this set of samples, a paired sample $t$ test was carried out. No statistical differences at the 95% of confidence interval between the intradermal and collected ISF values were found


https://doi.org/10.1021/acssensors.3c02086
ACS Sens. 2024, 9, 361−370

**Table 1. Results in the Ex Vivo Analysis Utilizing Pieces of Rat Skin**[a]

| | conditioning solution | | $CO_2$−MN patch | | | reference method | | | differences (%) | | |
|---|---|---|---|---|---|---|---|---|---|---|---|
| skin sample | pH | $CO_3^{2-}$ ($\mu$M) | pH[b] | $CO_3^{2-}$ ($\mu$M)[c] | $CO_2$ (mM)[d] | pH | $CO_3^{2-}$ ($\mu$M) | $CO_2$ (mM) | pH | $CO_3^{2-}$ | $CO_2$ |
| 1 | 7.96 | 200 | 8.05 | 247.3 | 0.5 | 8.0 | ND | <0.2[e] | | 0.6 | |
| 2 | 7.72 | 90 | 7.72 | 59.3 | 0.8 | 7.73 | 72.1 | 0.8 | 0.1 | 17.8 | 0 |
| 3 | 7.71 | 90 | 7.69 | 80.9 | 1.2 | 7.78 | 90.9 | 1.0 | 1.2 | 11.0 | 20.0 |
| 4 | 7.35 | 50 | 7.43 | 49.6 | 2.4 | 7.51 | 58.1 | 2.3 | 1.1 | 14.6 | 4.3 |
| 5 | 7.04 | 10 | 6.94 | 8.8 | 4.1 | 7.03 | 10.2 | 3.5 | 1.2 | 13.7 | 17.1 |
| 6 | 6.95 | 10 | 7.03 | 2.1 | 6.2 | ND | ND | ND | | | |

[a]ND = non detecting content, because the collected volume of the ISF was not enough to perform the measurements. [b]Ultra-micro pH-meter. [c]$CO_3^{2-}$−MN. [d]Calculated from pH and $CO_3^{2-}$ measurements. [e]i-Stat Abbott ($PCO_2$ < 5 mmHg).

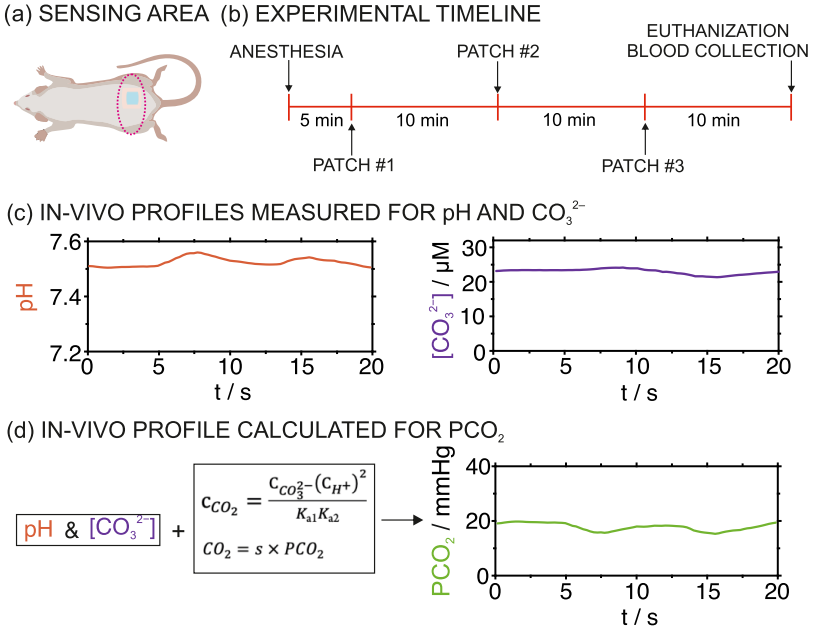


**Figure 6.** In vivo measurements in rats with the $CO_2$−MN patch. (a) Sensing zone. (b) Experimental timeline. (c) Dynamic profiles for pH and $CO_3^{2-}$ obtained in rat no. 2 at 15 min from the anesthesia. (d) The $PCO_2$ profile calculated from pH, $CO_3^{2-}$, eqs 1 and 2.

for pH ($p$ = 0.19), and $CO_2$ ($p$ = 0.18). Then, the ISF sample collected from skin #1 was the only one analyzed with the ABG device, providing a value of $PCO_2$ < 5 mmHg that approximately corresponds to a $CO_2$ concentration <0.15 mM. The precision for such a value was not enough to be quantitatively compared with the results provided by the $CO_2$−MN patch (0.5 mM) since it was below the limit of detection of the ABG device. Regarding skin #6, an extremely low volume of ISF (<5 $\mu$L) was extracted, hence precluding its analysis. Overall, the accuracy of the intradermal measurements using the $CO_2$−MN results in the *ex vivo* approach showed suitability for further animal-based tests, in particular, with anesthetized rats.

**In Vivo $CO_2$ Measurements in Anesthetized Rats.** The developed $CO_2$−MN patch was used for in vivo monitoring of $CO_2$ levels in the ISF of five anesthetized rats. Details about the experiments, protocols, and ethical permit are provided in the Experimental Section and Supporting Information. In essence, the $CO_2$−MN patch was connected to the portable multipotentiometric board inside the casing and calibrated. Once the rat was successfully anesthetized and positioned in the assay platform (ca. 5 min after the initiation of the anesthesia), the MNs were manually inserted into the lower part of the back of the rat (Figure 6a), which was previously shaved (Figures 2e and S2b), and transdermal measurements for ca. 2 min were allowed. The entire assay lasted ca. 40 min for each rat, with discrete measurements performed at ca. every 10 min with different patches. The experimental timeline is illustrated in Figure 6b. After the on-body measurements, the rat was physically euthanized, and samples containing a mixture of arterial-venous blood were collected and analyzed with the blood gas analyzer device immediately after collection and after 3 h (to discard any change in $PCO_2$ due to atmospheric equilibration, Supporting Information and Table S7).

Figure 6c depicts the dynamic pH and $CO_3^{2-}$ concentration profiles obtained for rat 1, as an example. The combination of these two by considering eq 1 provides the dynamic $CO_2$ concentration. Additionally using eq 2 and the appropriate solubility product (Supporting Information), the $PCO_2$ profile can be estimated (Figure 6d). Then, to investigate if these measurements correlate with the traditional blood gas test, discrete data points for pH, bicarbonate ($HCO_3^-$), and $PCO_2$ were calculated by averaging 20 s of the entire responses provided by the pH− and $CO_3^{2-}$−MNs (i.e., portions of stable signal occurring after the initial response time of the MNs, ca. 30 s after the measurement initiation, were selected). Then, in addition to $PCO_2$ and pH values, the blood gas analyzer displays the $HCO_3^-$ levels; therefore, these were also calculated from the MNs for comparison purposes. While


https://doi.org/10.1021/acssensors.3c02086
ACS Sens. 2024, 9, 361−370

Table 2. Results in the In Vivo Analysis in Five Anesthetized Rats[a]

| | | ISF | | | | | blood | | |
|---|---|---|---|---|---|---|---|---|---|
| rat no. | patch number/time (min)[b] | pH | $CO_3^{2-}$ ($\mu$M) | $HCO_3^-$ (mM) | $CO_2$ (mM) | $PCO_2$ (mmHg) | pH | $HCO_3^-$ (mM) | $PCO_2$ (mmHg) |
| 1 | 1/15 | 7.52 ± 0.02 | 23.0 ± 0.7 | 10.8 ± 0.5 | 0.5 ± 0.04 | 17.3 ± 1.3 | 7.7 | 23.1 | 18.8 |
| | 2/25 | 7.61 ± 0.07 | 45.1 ± 0.9 | 18.3 ± 0.1 | 0.6 ± 0.1 | 18.8 ± 2.3 | | | |
| | 3/35 | 7.78 ± 0.12 | 138.2 ± 0.3 | 18.6 ± 0.8 | 0.5 ± 0.1 | 10.5 ± 1.9 | | | |
| 2 | 4/15 | 7.27 ± 0.05 | 21.3 ± 1.3 | 25.3 ± 0.9 | 1.4 ± 0.1 | 45.8 ± 4.3 | 7.3 | 14.0 | 48.8 |
| | 5/25 | 7.17 ± 0.04 | 16.1 ± 0.3 | 22.0 ± 1.6 | 1.6 ± 0.3 | 62.5 ± 0.6 | | | |
| | 6/35 | 7.24 ± 0.02 | 18.6 ± 0.4 | 20.7 ± 1.1 | 1.4 ± 0.1 | 49.8 ± 1.9 | | | |
| 3 | 7/15 | 7.39 ± 0.03 | 28.8 ± 2.2 | 23.3 ± 0.9 | 1.2 ± 0.8 | 39.3 ± 2.5 | 7.4 | 29.8 | 53.7 |
| | 8/25 | 7.17 ± 0.04 | 30.6 ± 1.9 | 23.3 ± 3.9 | 2.2 ± 0.3 | 73.6 ± 9.7 | | | |
| | 9/35 | 7.33 ± 0.02 | 22.8 ± 0.8 | 21.1 ± 0.5 | 1.2 ± 0.02 | 41.2 ± 0.7 | | | |
| 4 | 10/35 | 7.21 ± 0.13 | 2.8 ± 0.8 | 2.9 ± 0.5 | 0.2 ± 0.02 | 7.5 ± 0.6 | 7.5 | 27.6 | 23.9 |
| 5 | 11/25 | 7.22 ± 0.18 | 22.6 ± 0.2 | 13.1 ± 0.8 | 0.9 ± 0.02 | 29.8 ± 0.5 | 7.6 | 25.7 | 25.4 |
| | 12/35 | 7.56 ± 0.02 | 45.1 ± 0.02 | 18.3 ± 0.4 | 0.7 ± 0.02 | 25.4 ± 0.7 | | | |

[a]ND = nondetecting content, because the collected volume of the ISF was not enough to perform the measurements. [b]Approximated time after anesthesia at which the corresponding on-body measurement was performed.

$PCO_2$ is mainly balanced by the respiratory system and gives information related to patient's ventilation, $HCO_3^-$ is mainly regulated by the kidney, and indicates the presence of metabolic disorders. Altogether may provide valuable clinical insight about acid−base disturbances.[32] The reader is kindly referred to the Supporting Information about $HCO_3^-$calculations performed herein from the experimental data.

Table 2 shows the results for the in vivo measurements performed with the six rats together with those observed in the blood gas test. In ISF, excluding the data in rat no. 4, pH values ranged from 7.2 to 7.8, $HCO_3^-$ from 11 to 25 mM, and $PCO_2$ from 10 to 74 mmHg. In blood, pH values ranged from 7.3 to 7.7, $HCO_3^-$ from 14.0 to 30 mM, and $PCO_2$ from 19 to 54 mmHg. In principle, ISF and blood ranges were rather coincidental and within the expected clinical levels (Table S7). Therefore, further correlation and statistical analyses were performed, except for the data from rat no. 4 that presented a high difference between ISF-blood results.

Figure S8a presents the correlation observed for ISF and blood $PCO_2$, which is the main target analyte herein, as an example. The Pearson correlation coefficients for the relationships between ISF and blood values for pH, $HCO_3^-$ and $PCO_2$ ($n$ = 11 for each parameter) were found to be 0.91, 0.74, and 0.86. A positive correlation between both biofluids (considering a threshold of 0.75) was revealed for pH and $PCO_2$, while it was less evident for $HCO_3^-$. Analogously, the results from a paired $t$ test for pH and $PCO_2$ parameters pointed out no statistically significant differences (95% confidence interval) between both biofluids ($p$ = 0.07 for pH and $p$ = 0.97 for $PCO_2$). Statistical differences were observed for the bicarbonate ($p$ = 0.02). Notably, $HCO_3^-$ concentrations were obtained by calculations with both techniques (MNs and i-Stat). For the i-Stat, it has been reported that the provided levels may differ from reality,[33] which would explain the differences found with the MNs.

Figure S8b presents the Bland-Altman analysis carried out for the ISF-blood $PCO_2$ ($n$ = 11), suggesting a minor bias (the mean difference between the 2 methods) of 0.1 mmHg, with an acceptable precision (SD of the differences) of 10.3 mmHg. The 95% lower and upper limits of agreement were −20.0 and 20.1 mmHg, respectively, englobing all of the samples. A high number of samples showed differences >4.5 or 7.5 mmHg: 45% were ≤4.5 mmHg and 64% ≤ 7.5 mmHg. Only 36% of the measurements were outside the clinically acceptable range (±7.5 mmHg), as recommended by the American Association for Respiratory Care Therapists.[34]

It is important to mention that the statistical analysis was performed comparing ISF $PCO_2$ at different time points from the anesthesia (ca. 15, 25, and 35 min) with blood $PCO_2$ obtained after ca. 40 min from the anesthesia, which is not an ideal situation but that was adopted for practicality reasons. In an ideal scenario, blood samples would have been collected 10 min prior to each on-body measurement in ISF to be more comparable between them. Although venous blood sampling from the dorsal pedal vein was performed in our experiments between each interval of the on-body measurements with the patch, insufficient blood volume for analysis with the blood gas analyzer was extracted. This was due to the decrease of blood flow in the rat caused by the anesthesia.[35]

Also, $PCO_2$ is a dynamic physiological parameter: changes in ISF along the entire assay may be attributed to natural fluctuations in the animal as well as as a consequence of the anesthesia conditions. For example, a decrease in the pH from 7.4 to 7.2 connected to an increment of $PCO_2$ from ca. 30 to 40 mmHg has been reported in rodents under isoflurane anesthesia for 45 min. Accordingly, it seems logical to compare the values for ISF measurements (except for rat no. 4) at 35 min from the anesthesia with the arterial-venous blood values herein collected, as these are the data closer in time. A paired $t$ test ($n$ = 4) revealed no statistically significant differences between ISF and blood $PCO_2$ ($p$ = 0.21).

Overall, our results demonstrated not only the possibility of performing accurate intradermal $CO_2$ measurements but also a promising correlation between ISF and blood $PCO_2$. Despite the auspicious outcomes, we believe important to discuss some aspects useful to advance the analytical reliability and technological readiness of the herein developed patch. Regarding the correlation between ISF and blood measurements: (i) To the best of our knowledge, there are no previous reports on correlations between ISF and blood $CO_2$. However, a correlation seems to be expected, which is endorsed by existing relationships between both arterial and venous $CO_2$ with transcutaneous values.[8] In any case, a lag time of ca. 10 min should manifest. (ii) Shorter or larger differences have been reported for blood and transcutaneous $CO_2$ depending


https://doi.org/10.1021/acssensors.3c02086
ACS Sens. 2024, 9, 361−370

on the measurement position (e.g., earlobe, chest, and arm/forearm).[34] (iii) Arterial and venous $CO_2$ levels correlate between them and hence, mixed blood samples may be an alternative when arterial and/venous blood collection are not feasible, as in our experiments. (iv) The existence of a physiological disagreement between ISF and blood could be possible. Notably, dermal $CO_2$ concentrations come from blood diffusion but also $CO_2$ production by the tissues, in analogy to transcutaneous $CO_2$.[2,5] Accordingly, at some point, it would be convenient to directly study the relationship between ISF $CO_2$ levels and the clinical conditions of interest.

Considering the $CO_2$ values provided by the MN patch, several calculations are needed to translate the pH and $CO_3^{2-}$ measurements into $PCO_2$, which incorporate summative errors into the outcomes. Importantly, the $K_a$ values needed to operate eq 1 may change with certain (physio)pathological conditions due to changes in the temperature, ionic strength, and others. The same applies to the solubility product in eq 2, indeed we used that reported for blood and assuming the same value for ISF. On the one hand, calculations will benefit from temperature-based corrections using an MN sensor that could be additionally implemented in the patch. Not only the constants but also the potentiometric slope of the MN sensors could be improved. On the other hand, when performing MN-based measurements in the clinical context in the near future, it would be convenient to look for relationships between pH/$CO_3^{2-}$ levels with the health conditions rather than $CO_2$, to reduce calculations. Alternatively, a $HCO_3^-$ sensor could be used instead of the $CO_3^{2-}$ one due to the larger levels in blood and thus in ISF.

## CONCLUSIONS

We developed an MN-based analytical platform for detecting $CO_2$ levels in ISF based on transdermal pH and $CO_3^{2-}$ measurements. The adequate analytical performances demonstrated at the in vitro level for the pH− and $CO_3^{2-}$−MN sensors inspired the monitoring of $CO_2$ levels in environmentally controlled chambers to validate the needed calculations. Then, ex vivo assays proved the suitability of the $CO_2$−MN patch, in terms of resiliency and accuracy. Furthermore, coupling the patch with a portable potentiometer wirelessly connected to a mobile phone for data visualization allowed for in vivo studies in anesthetized rats. Preliminary studies of the correlation between ISF and blood $CO_2$ were performed, revealing very interesting prospects. The results herein presented have a great potential for $CO_2$ analysis inside organs such as the skin of animals and humans, but also, it could be applied for other tissues and beings (e.g., plants), where $CO_2$ monitoring is relevant.

## ASSOCIATED CONTENT

### Supporting Information

The Supporting Information is available free of charge at https://pubs.acs.org/doi/10.1021/acssensors.3c02086.

Experimental details; procedures for in vivo tests; pictures of the system; SEM images; reproducibility; selectivity; and drift (PDF)

## AUTHOR INFORMATION


### Corresponding Authors

**Gastón A. Crespo** − *Department of Chemistry, KTH Royal Institute of Technology, SE-114 28 Stockholm, Sweden; UCAM-SENS, Universidad Católica San Antonio de Murcia, UCAM HiTech, 30107 Murcia, Spain;* orcid.org/0000-0002-1221-3906; Email: gacp@kth.se

**María Cuartero** − *Department of Chemistry, KTH Royal Institute of Technology, SE-114 28 Stockholm, Sweden; UCAM-SENS, Universidad Católica San Antonio de Murcia, UCAM HiTech, 30107 Murcia, Spain;* orcid.org/0000-0002-3858-8466; Email: mariacb@kth.se

### Authors

**Águeda Molinero-Fernandez** − *Department of Chemistry, KTH Royal Institute of Technology, SE-114 28 Stockholm, Sweden; UCAM-SENS, Universidad Católica San Antonio de Murcia, UCAM HiTech, 30107 Murcia, Spain*

**Qianyu Wang** − *Department of Chemistry, KTH Royal Institute of Technology, SE-114 28 Stockholm, Sweden*

**Xing Xuan** − *Department of Chemistry, KTH Royal Institute of Technology, SE-114 28 Stockholm, Sweden; UCAM-SENS, Universidad Católica San Antonio de Murcia, UCAM HiTech, 30107 Murcia, Spain*

**Åsa Konradsson-Geuken** − *Section of Neuropharmacology and Addiction Research, Department of Pharmaceutical Biosciences, Uppsala University, Uppsala 753 10, Sweden*

Complete contact information is available at: https://pubs.acs.org/10.1021/acssensors.3c02086


### Author Contributions

All authors have given approval to the final version of the manuscript.

### Notes

The authors declare no competing financial interest.

## ACKNOWLEDGMENTS

The authors acknowledge the financial support from the Region of Stockholm (SLL20200947), Stiftelsen Olle Engkvist Byggmästare (204-0214), and Swedish Research Council (VR-2019-04142). A.M-F. and M.C. acknowledge the Carl Tryggers Stiftelse (CTS 20:88). Q.W. gratefully thanks the China Scholarship Council for supporting his PhD studies. The authors acknowledge Uppsala University Behavior Facility (UUBF) for the rat-based assays. They thank E. Ekelund for his support with the board, as well as J. Dillner and R. Merino for their contributions in the settings of the project from a clinical perspective.

## REFERENCES

(1) Gattinoni, L.; Pesenti, A.; Matthay, M. Understanding Blood Gas Analysis. *Intensive Care Med.* **2018**, *44*, 91−93.

(2) Sankaran, D.; Zeinali, L.; Iqbal, S.; Chandrasekharan, P.; Lakshminrusimha, S. Non-Invasive Carbon Dioxide Monitoring in Neonates: Methods, Benefits, and Pitfalls. *J. Perinatol.* **2021**, *41* (11), 2580−2589.

(3) Higgins, C. Capillary Blood Gases: To Arterialize or Not. *MLO Med. Lab Obs* **2008**, *40* (42), 44−47.

(4) Sood, P.; Paul, G.; Puri, S. Interpretation of Arterial Blood Gas. *Indian J. Crit. Care Med.* **2010**, *14* (2), 57−64.

(5) Dervieux, E.; Théron, M.; Uhring, W. Carbon Dioxide Sensing—Biomedical Applications to Human Subjects. *Sensors* **2022**, *22* (1), 188−233, DOI: 10.3390/s22010188.

(6) Friedel, M.; Thompson, I. A. P.; Kasting, G.; Polsky, R.; Cunningham, D.; Soh, H. T.; Heikenfeld, J. Opportunities and challenges in the diagnostic utility of dermal interstitial fluid. *Nat. Biomed Eng.* **2023**, *7*, 1541−1555, DOI: 10.1038/s41551-022-00998-9.

(7) Escalante-Kanashiro, R.; Tantaleán-Da-Fieno, J. Capillary Blood Gases in a Pediatric Intensive Care Unit. *Crit. Care Med.* **2000**, *28* (1), 224−226.
(8) Treger, R.; Pirouz, S.; Kamangar, N.; Corry, D. Agreement between Central Venous and Arterial Blood Gas Measurements in the Intensive Care Unit. *Clin. J. Am. Soc. Nephrol.* **2010**, *5* (3), 390−394.
(9) Eberhard, P. The Design, Use, and Results of Transcutaneous Carbon Dioxide Analysis: Current and Future Directions. *Anesth. Analg.* **2007**, *105* (6), S48−S52.
(10) García-Guzmán, J. J.; Pérez-Ràfols, C.; Cuartero, M.; Crespo, G. A. Toward in Vivo Transdermal pH Sensing with a Validated Microneedle Membrane Electrode. *ACS Sens.* **2021**, *6* (3), 1129−1137.
(11) Parrilla, M.; Cuartero, M.; Sánchez, S. P.; Rajabi, M.; Roxhed, N.; Niklaus, F.; Crespo, G. A. Wearable All-Solid-State Potentiometric Microneedle Patch for Intradermal Potassium Detection. *Anal. Chem.* **2019**, *91* (2), 1578−1586.
(12) Wang, Q.; Molinero-Fernandez, A.; Casanova, A.; Titulaer, J.; Campillo-Brocal, J. C.; Konradsson-Geuken, Å.; Crespo, G. A.; Cuartero, M. Intradermal Glycine Detection with a Wearable Microneedle Biosensor: The First In Vivo Assay. *Anal. Chem.* **2022**, *94* (34), 11856−11864.
(13) Wu, Y.; Tehrani, F.; Teymourian, H.; Mack, J.; Shaver, A.; Reynoso, M.; Kavner, J.; Huang, N.; Furmidge, A.; Duvvuri, A.; Nie, Y.; Laffel, L. M.; Doyle, F. J.; Patti, M. E.; Dassau, E.; Wang, J.; Arroyo-Currás, N. Microneedle Aptamer-Based Sensors for Continuous, Real-Time Therapeutic Drug Monitoring. *Anal. Chem.* **2022**, *94* (23), 8335−8345.
(14) Molinero-Fernández, Á.; Casanova, A.; Wang, Q.; Cuartero, M.; Crespo, G. A. In Vivo Transdermal Multi-Ion Monitoring with a Potentiometric Microneedle-Based Sensor Patch. *ACS Sens.* **2023**, *8* (1), 158−166.
(15) Goud, K. Y.; Mahato, K.; Teymourian, H.; Longardner, K.; Litvan, I.; Wang, J. Wearable Electrochemical Microneedle Sensing Platform for Real-Time Continuous Interstitial Fluid Monitoring of Apomorphine: Toward Parkinson Management. *Sens. Actuators, B* **2022**, *354*, 131234−131242.
(16) Müller, M.; Cascales, J. P.; Marks, H. L.; Wang-Evers, M.; Manstein, D.; Evans, C. L. Phosphorescent Microneedle Array for the Measurement of Oxygen Partial Pressure in Tissue. *ACS Sens.* **2022**, *7*, 3440−3449.
(17) https://www.matweb.com/search/datasheet.aspx?matguid=a616c157e8b5424994a30d1d455373e3&ckck=1.
(18) https://www.matweb.com/search/DataSheet.aspx?MatGUID=589efb062abe4ee7bdbe10fd64f55590.
(19) Kruse, J. A. Calculation of Plasma Bicarbonate Concentration *versus* Measurement of Serum $CO_2$ Content. PK′ Revisited. *Clin. Intensive Care* **1995**, *6*, 15−20.
(20) Cuartero, M.; Pankratova, N.; Cherubini, T.; Crespo, G. A.; Massa, F.; Confalonieri, F.; Bakker, E. In Situ Detection of Species Relevant to the Carbon Cycle in Seawater with Submersible Potentiometric Probes. *Environ. Sci. Technol. Lett.* **2017**, *4*, 410−415.
(21) Athavale, R.; Pankratova, N.; Dinkel, C.; Bakker, E.; Wehrli, B.; Brand, A. Fast Potentiometric CO2 Sensor for High-Resolution in Situ Measurements in Fresh Water Systems. *Environ. Sci. Technol.* **2018**, *52*, 11259−11266.
(22) Chesler, M.; Chen, J. C. T.; Kraig, R. P. Determination of Extracellular Bicarbonate and Carbon Dioxide Concentrations in Brain Slices Using Carbonate and PH-Selective Microelectrodes. *J. Neurosci. Methods* **1994**, *53*, 129.
(23) Wietasch, K.; Kraig, R. P. Carbonic Acid Buffer Species Measured in Real Time with an Intracellular Microelectrode Array. *Am. J. Physiol.: Regul., Integr. Comp. Physiol.* **1991**, *261*, R760−R765.
(24) García-Guzmán, J. J.; Pérez-Ràfols, C.; Cuartero, M.; Crespo, G. A. Microneedle Based Electrochemical (Bio)Sensing: Towards Decentralized and Continuous Health Status Monitoring. *TrAC, Trends Anal. Chem.* **2021**, *135*, No. 116148.
(25) *CRC Handbook of Chemistry and Physics*; Haynes, W. M.; Lide, D. R.; Bruno, T. J., Eds.; CRC Press, 2016.
(26) Dervisevic, M.; Dervisevic, E.; Esser, L.; Easton, C. D.; Cadarso, V. J.; Voelcker, N. H. Wearable Microneedle Array-Based Sensor for Transdermal Monitoring of PH Levels in Interstitial Fluid. *Biosens. Bioelectron.* **2023**, *222*, No. 114955.
(27) Bakker, E.; Pretsch, E.; Bühlmann, P. Selectivity of Potentiometric Ion Sensors. *Anal. Chem.* **2000**, *72* (6), 1127−1133.
(28) Murray, C. D.; Hastings, A. B. The maintenance of carbonic acid equilibrium in the body. *J. Biol. Chem.* **1925**, *65*, 265−278, DOI: 10.1016/s0021-9258(18)84891-8.
(29) U. S. FDA. Bioanalytical Method Validation Guidance for Industry. US Department of Health and Human Services Food and Drug Administration Center for Drug Evaluation and Research and Center for Veterinary Medicine.. 2018.
(30) EMA ICH. Q2 (R2) Validation of Analytical Procedures—Scientific Guideline.
(31) Severinghaus, J. W.; Bradley, A. F. Electrodes for Blood PO2 and PCO2 Determination. *J. Appl. Physiol.* **1958**, *13*, 515−520.
(32) Fauci, A. S. *Harrison's Principles of Internal Medicine*; McGraw-Hill Education, 2015.
(33) Saleem, M.; Dimeski, G.; Bourne, L.; Coates, P. Artifactually Elevated Serum Bicarbonate Results Caused by Elevated Serum Lactate Dehydrogenase Concentrations. *Ann. Clin. Biochem.: Int. J. Lab. Med.* **2013**, *50*, 365−367.
(34) Conway, A.; Tipton, E.; Liu, W.-H.; Conway, Z.; Soalheira, K.; Sutherland, J.; Fingleton, J. Accuracy and Precision of Transcutaneous Carbon Dioxide Monitoring: A Systematic Review and Meta-Analysis. *Thorax* **2019**, *74*, 157.
(35) Shumkova, V.; Sitdikova, V.; Rechapov, I.; Leukhin, A.; Minlebaev, M. Effects of Urethane and Isoflurane on the Sensory Evoked Response and Local Blood Flow in the Early Postnatal Rat Somatosensory Cortex. *Sci. Rep.* **2021**, *11*, No. 9567, DOI: 10.1038/s41598-021-88461-8.


https://doi.org/10.1021/acssensors.3c02086
*ACS Sens.* 2024, 9, 361−370